Supporting Information

Single-phase ultrathin holey nanoflower Ni_5P_4 as bifunctional electrocatalyst for efficient water splitting

Lihua Yao[a,1], Zhuo Qiu[a,1], Xingliang Yin[b], Ying Yang[a], Xiaodi Hong[a], Zhi Yang[a,*]

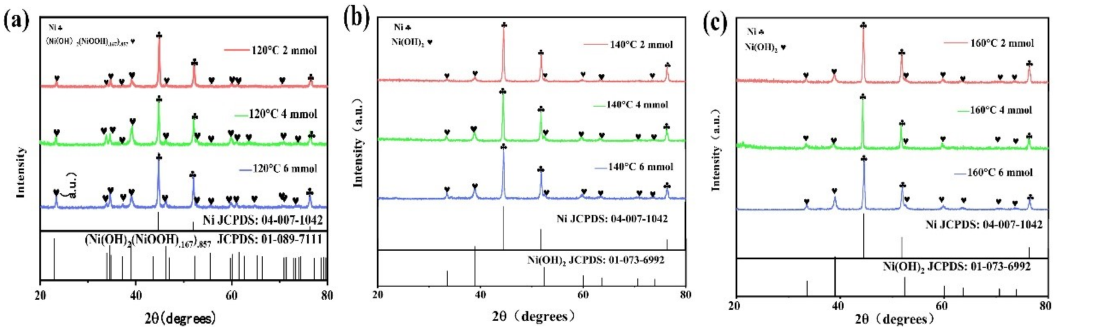

Fig.S1. XRD of precursor of Nickel phosphide which prepared with different concentrations of $Ni(NO_3)_2 \cdot 6H_2O$ (2, 4, 6 mmol), (a) hydrothermal temperatures 120 °C; (b) hydrothermal temperatures 140 °C; (c) hydrothermal temperatures 160 °C.

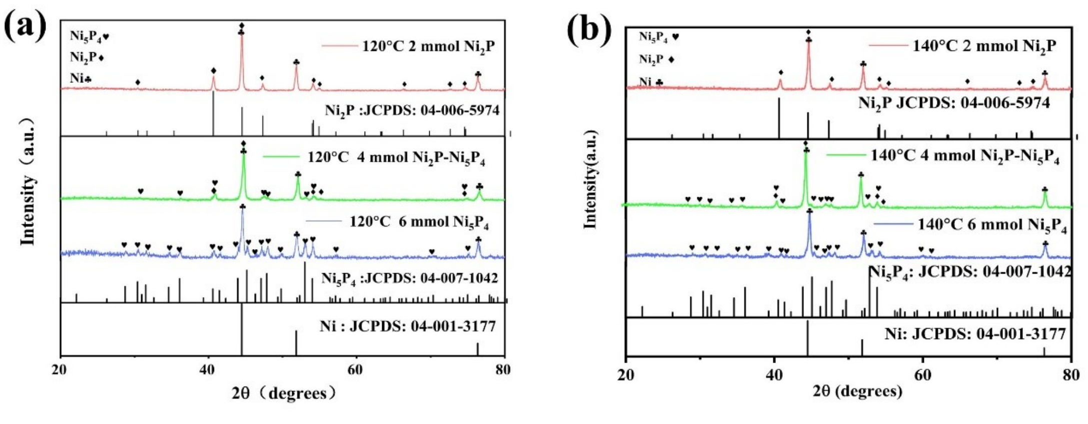

Fig. S2. XRD of Nickel phosphide that of precursor was prepared with different concentrations of $Ni(NO3)_2 \cdot 6H_2O$ (2, 4, 6mmol) and different hydrothermal temperature, (a) hydrothermal temperatures 120 °C; (b) hydrothermal temperatures 140 °C.

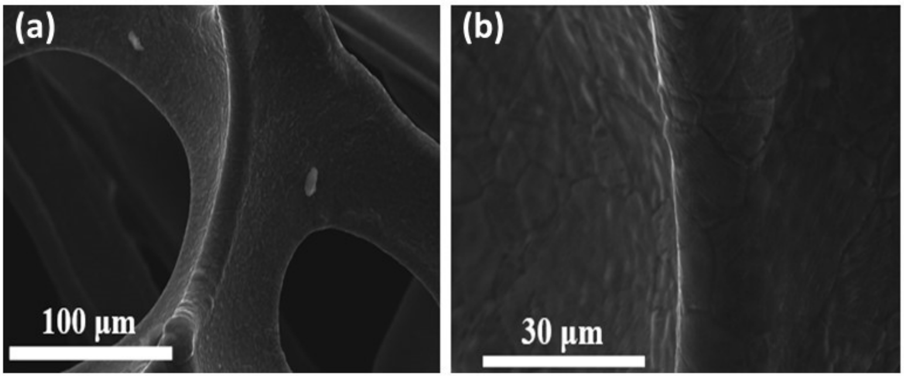

Fig. S3 (a) (b) SEM images of the NF.

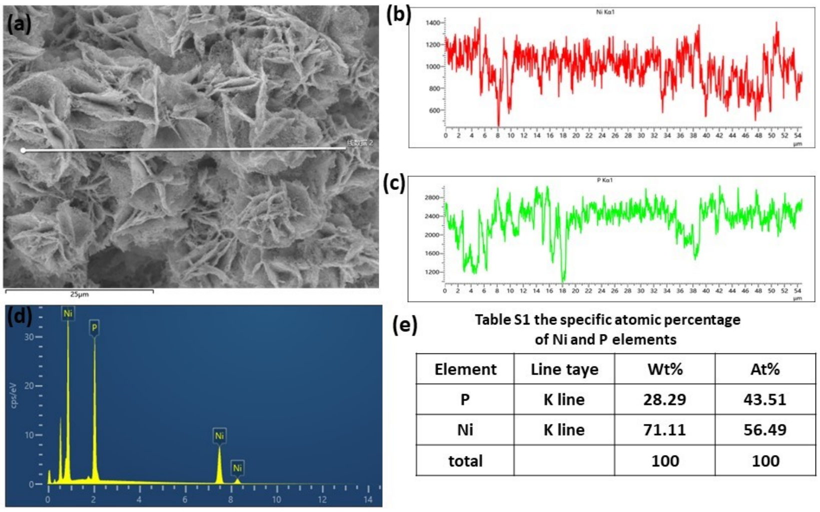

Table S1 the specific atomic percentage of Ni and P elements

Element	Line taye	Wt%	At%
P	K line	28.29	43.51
Ni	K line	71.11	56.49
total		100	100

Fig. S4. (a b c d**)** Energy Dispersive Spectrum (EDS) of 3D SHF-Ni_5P_4; (e) The specific atomic percentage of Ni and P elements of 3D SHF-Ni_5P_4.

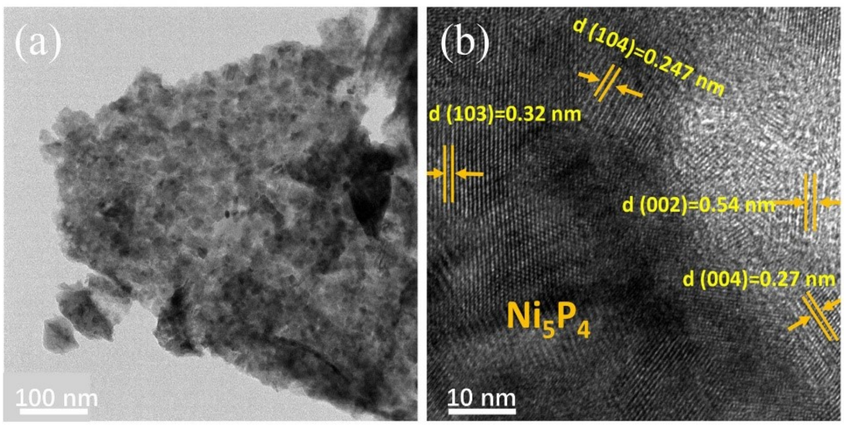

Fig. S5. TEM micrographs (a) of 3D SHF-Ni_5P_4; (c) HR-TEM image of 3D SHF-Ni_5P_4.

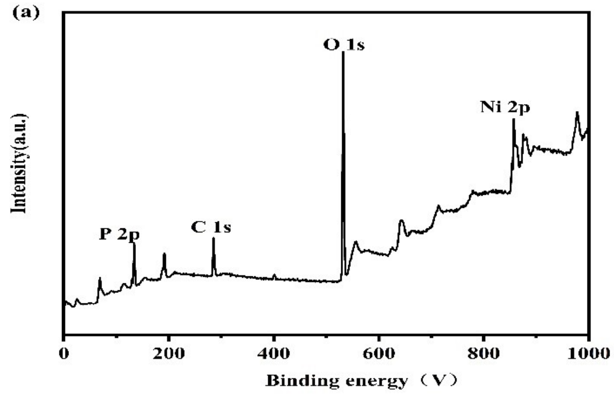

Fig. S6. A scan survey spectrum of 3D SHF-Ni_5P_4

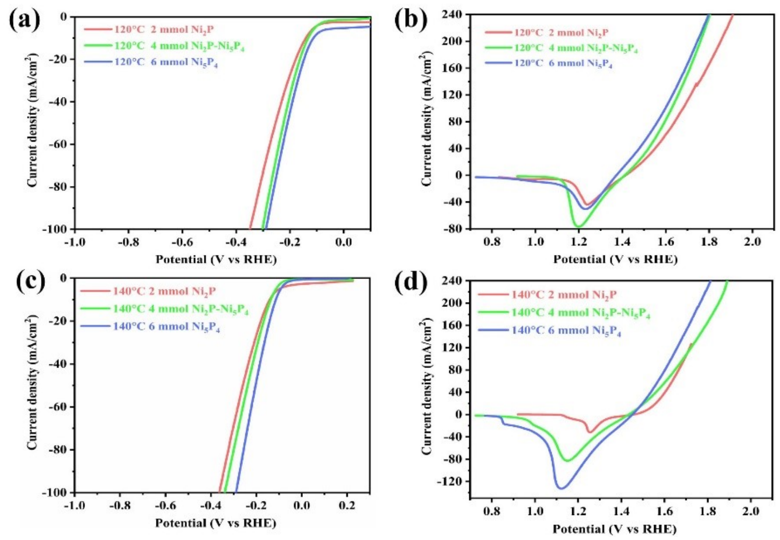

Fig.S7. LSV polarization curve of nickel phosphide that of the precursor prepared with 2mmol, 4mmol, and 6mmol of Ni(NO3)$_2$·6H_2O solution at the different temperature in hydrothermal process; (a),(b) HER and OER of nickel phosphide precursor were prepared at 120 °C; (c),(d) HER and OER of nickel phosphide precursor were prepared at 140 °C.

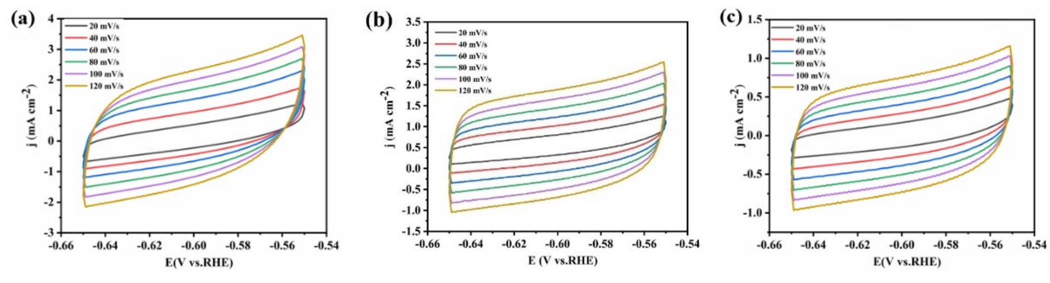

Fig. S8. OER CVs of (a) 3D SHF- Ni_5P_4; (b) Ni_5P_4-4; (c) Ni_5P_4-2 in 1 M KOH solution at scan rates of 20, 40, 60, 80, 100, and 120 mV/s, respectively.

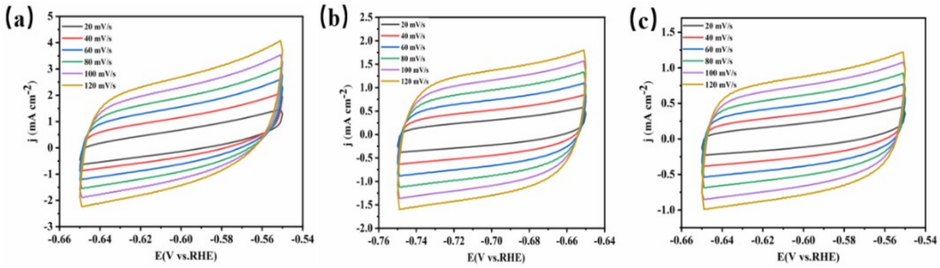

Fig. S9. HER CVs of (a) 3D SHF- Ni_5P_4; (b) Ni_5P_4-4; (c) Ni_5P_4-2 in 1 M KOH solution at scan rates of 20, 40, 60, 80, 100, and 120 mV/s, respectively.

Calculation of TOF values

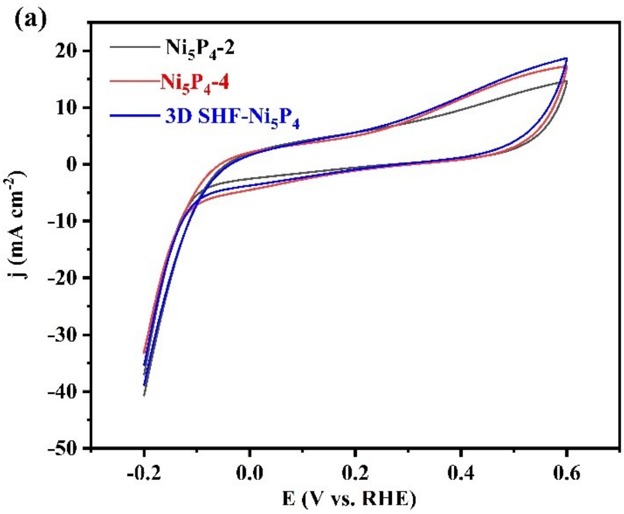

Fig. S10. (a) CV curves of Ni_5P_4-2、Ni_5P_4-4 and 3D SHF-Ni_5P_4 in 1.0 M KOH solution at a scan rate of 50 mV s^{-1}.

The TOF values are calculated via the following equation:

$$TOF = \frac{J}{mFn}$$

m: electrons are consumed to form one H_2 or O_2 molecule from water (2electrons for HER, 4 electrons for OER)

J (mA cm^{-2}): the current density at a fixed overpotential (OER 300mV, HER 200mV), during the LSV measurement in 1.0M KOH solution.

F: represents the Faraday constant (96485 C),

n: the total number of moles of active sites. The number of active sites (n) can be measured by a formerly reported method, n = Q/2F

Q: the cyclic voltametric charge capacity obtained by integrating the CV cures. The CV curve was tested in 1.0 M KOH solution at -0.2-0.6 V (vs. RHE) with a sweep rate of 50 mV s^{-1}.

For OER of 3D SHF-Ni_5P_4, determination of Turnover Frequency (TOF)

$$n = \frac{Q}{2F} = \frac{11.59}{2 \times 96485} = 6.01 \times 10^{-5}$$

$$TOF = \frac{J}{mFn} = \frac{65.54}{4 \times 96485 \times 6.01 \times 10^{-5}} = 2.83\ S^{-1}$$

Post electrolysis characterization

To gain further insight into the catalyst transformation following electrocatalysis, XRD, SEM, and XPS have been conducted to analyze 3D SHF- Ni_5P_4 after electrocatalytic stability test.

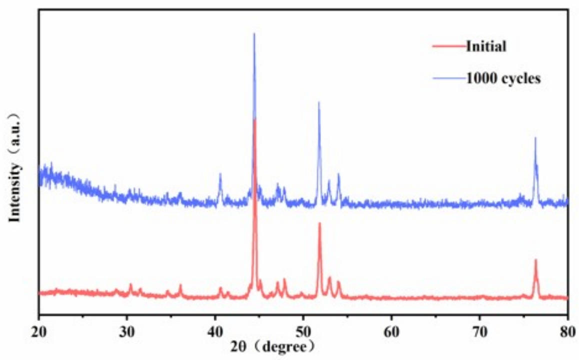

Fig. S11. The XRD spectra of 3D SHF- Ni_5P_4 for OER after 1000 cycles.

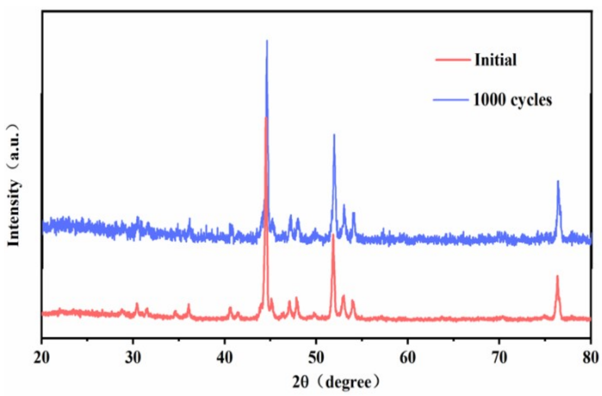

Fig. S12. The XRD spectra of 3D SHF- Ni_5P_4 for HER after 1000 cycles.

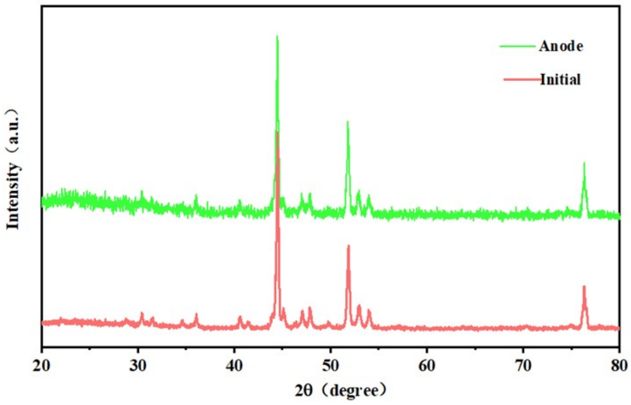

Fig. S13. The XRD spectra of 3D SHF-Ni_5P_4 as anode for water splitting after 24h.

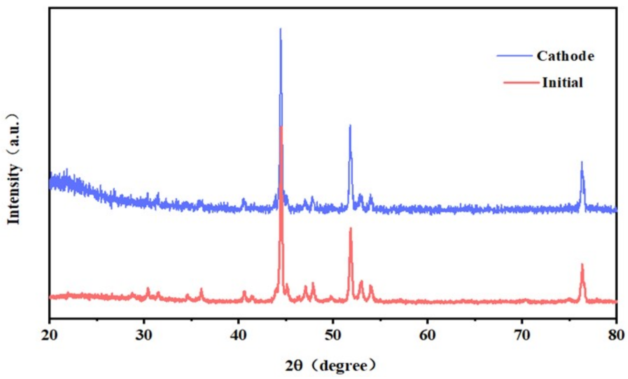

Fig. S14. The XRD spectra of 3D SHF- Ni_5P_4 as cathode for water splitting after 24 H.

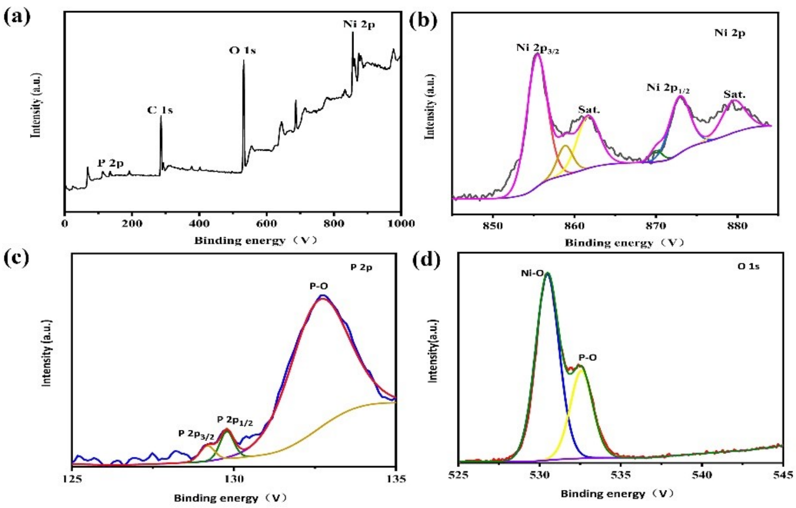

Fig. S15. XPS spectra of (a) a scan survey spectrum (b) Ni and (c) P after 22h of OER.

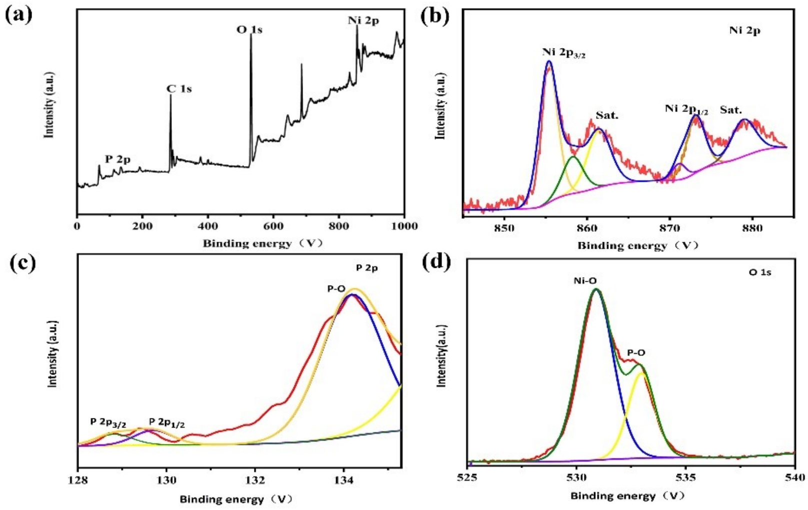

Fig. S16. XPS spectra of (a) a scan survey spectrum (b) Ni and (c) P after 22h of HER.

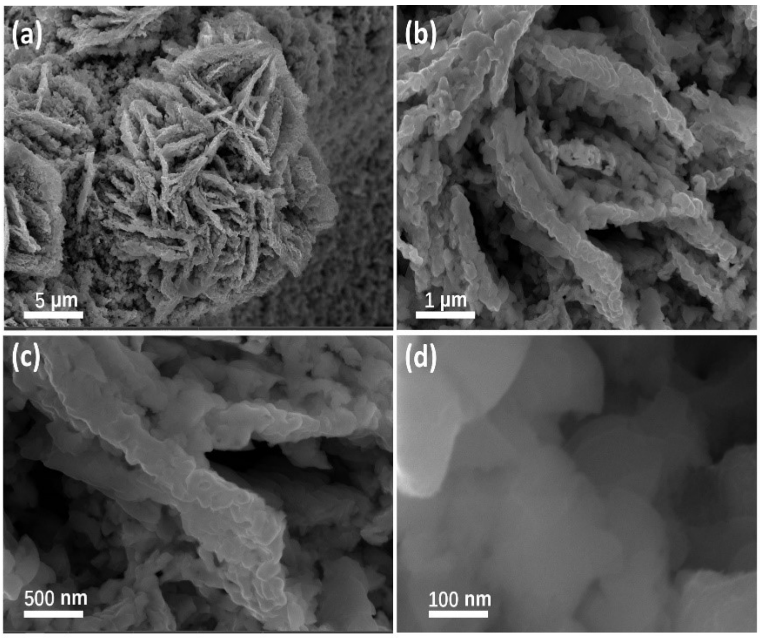

Fig. S17. (a-d) 3D SHF- Ni_5P_4 for OER after 1000 cycles.

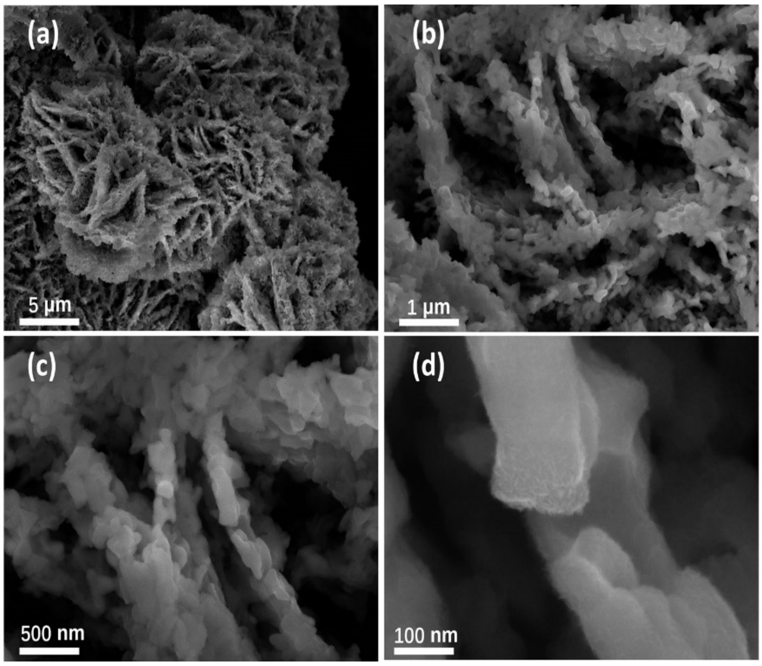

Fig. S18. (a-b) SEM of 3D SHF- Ni_5P_4 for HER after 1000 cycles.

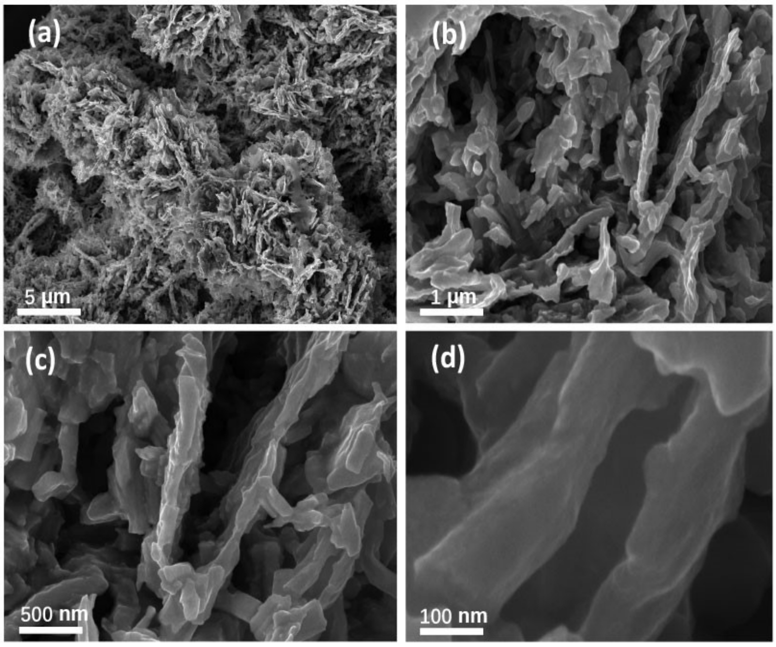

Fig. S19. (a-d) SEM of 3D SHF- Ni_5P_4 for OER after22h.

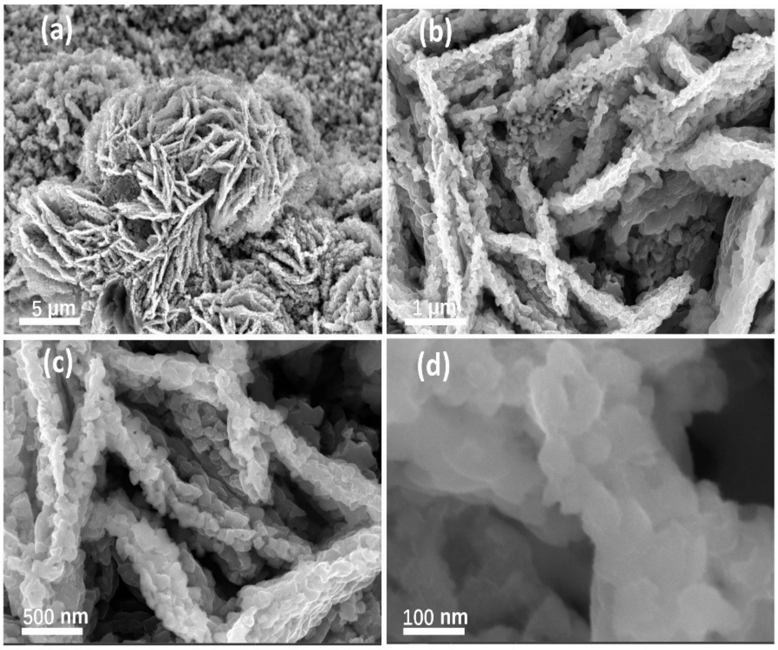

Fig. S20. (a-d) SEM of 3D SHF- Ni_5P_4 for HER after 22h.

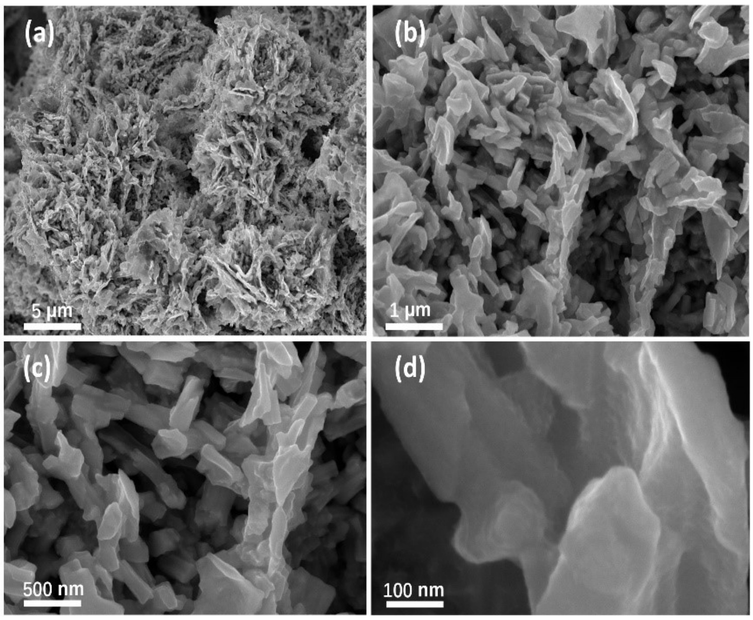

Fig. S21. (a-d) SEM of 3D SHF-Ni_5P_4 as anode for water splitting after 24h.

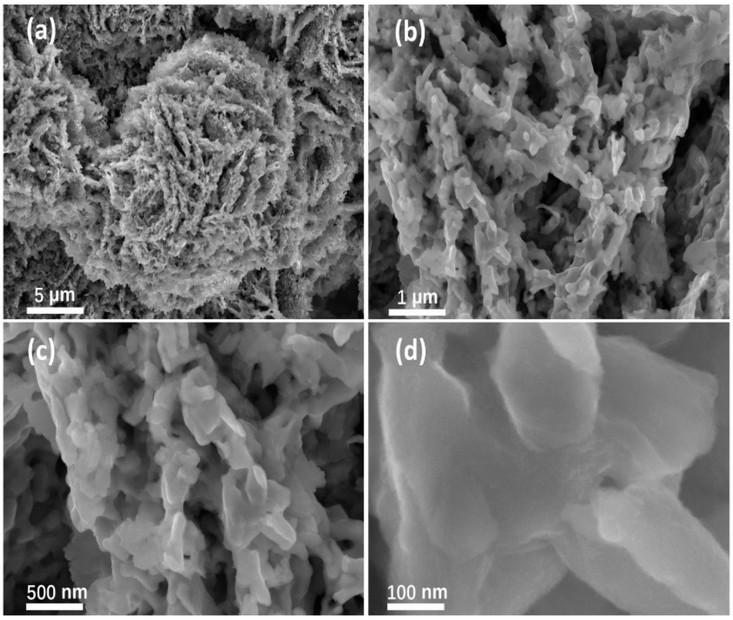

Fig. S22. (a-d) SEM of 3D SHF-Ni_5P_4 as cathode for water splitting after 24h.

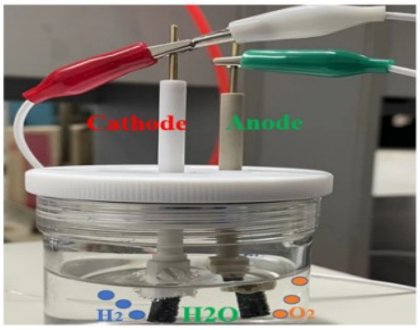

Fig. S23. Overall water splitting video and picture.

OER and HER mechanism in alkaline

Based on published articles, the mechanisms of OER and HER in alkaline are as follows:

(1) OER mechanism

The mechanism of OER is complicated and still debatable on the anode catalysts. The OER mechanism involves the adsorption and desorption of intermediates, i.e., $OH_{ads} \rightarrow O_{ads} \rightarrow OOH_{ads} \rightarrow O_{2ads}$ process (adsorbate evolution mechanism, AEM). The steps of OER primitives under alkaline conditions are as follows:

(1) $OH^- + * \rightarrow OH_{ads} + e^-$

(2) $OH_{ads} + OH^- \rightarrow O_{ads} + H_2O + e^-$

(3) $O_{ads} + OH^- \rightarrow OOH_{ads} + e^-$

(4) $2O_{ads} \rightarrow O_2 + *$

Overall: $4OH^- \rightarrow H_2O + O_2 + e^-$

Where the * represents the active sites on the catalyst surface, and the “ads” represents adsorbed state of intermediates (OH_{ads}, O_{ads}, OOH_{ads}, O_{2ads})

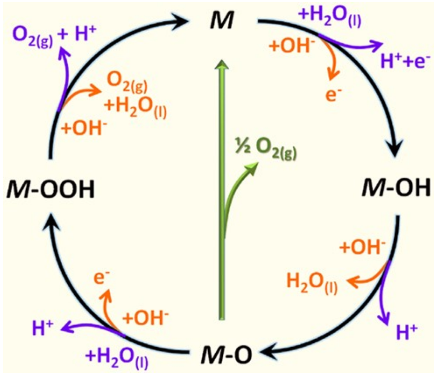

Fig. 1 Schematic diagram of OER mechanism[29]

(2) HER mechanism

In alkaline media, transition metal catalysts usually react with H2O and H^* to generate H_2.

the first step of HER is to generate H^* by reaction with H_2O. The second step is the rate-determining step(RDS), which depends ofn the activity of these catalysts.

The steps of HER primitives under alkaline conditions are as follows:

(1) $H_2O + e^- \rightarrow OH^- + H_{ads}$ (Volmer)

(2) $H_{ads} + H_2O + e^- \rightarrow OH^- + H_2$(Heyrovsky)

(3) $2H_{ads} \rightarrow H_2$(Tafel)

Where the * represents the active sites on the catalyst surface, and the “ads” represents adsorbed state of intermediates (H_{ads})

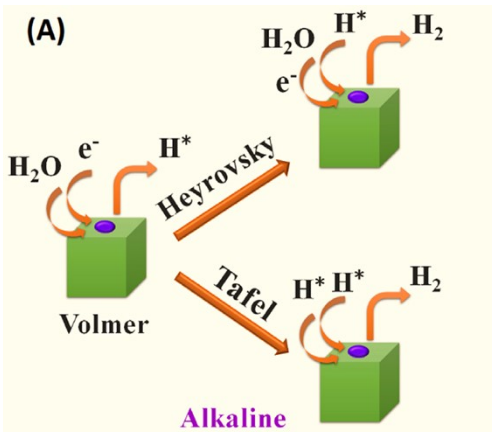

Fig. 2 Schematic diagram of HER mechanism in alkaline media[30]

According to reports, for HER reaction, the determination rate of the electrochemical reaction can be judged according to the Tafel slope of the reaction. When the Tafel slope is 120 mV dec^{-1}, the RDS is the Volmer process. When Tafel slope is 40 mV dec^{-1}, RDS is Heyrovsky process. RDS is a Tafel process when the Tafel slope is 30 mV dec^{-1}. In this work, there is no tafel slopes match the expected Tafel slopes of 30, 40, and 120 mV dec^{-1}, each of which correlate with a different rate-determining step of the HER. Although the Tafel analysis is useful in elucidating the rate-determining steps, too simplified discussion, fails to accurately describe the surface electrocatalysis. The relation between tafel slope and reaction mechanism will be studied in the next part of this work.

Table S2 Summary of various nickel phosphide catalytic electrodes for HER or OER

Catalyst	Activity	Current density (mA/cm2)	Potential	Electrolyte	Tafel slope (mV/dec)	Reference
3D SHF-Ni5P4	OER	10	180	1 M KOH	54	This work
	HER	10	106	1 M KOH	79.38	
N-C/Ni5P4/Fe3P	OER	10	252 mV	1 M KOH	24	[1]
Ni5P4 on Nickel foil	HER	10	140 mV	0.5MH2SO4		[2]
			150 mV	1 M KOH		
Ni5P4 -Ni2P-NS	HER	10	120 mV	0.5MH2SO4	79.1	[3]
CoP/ Ni5P4/CoP	HER	10	33 mV	0.5MH2SO4	43	[4]
Ni5P4/NF	HER	10	64 mV	1 M KOH	64	[5]
Ni5P4/NF	OER	10	182 mV	1 M KOH	58	[5]
Ni5P4@NiCo2O4	HER	10	27 mV	1 M KOH	27	[6]

S- Ni5P4 NPA/CP	HER	10	56 mV	1 M KOH	43.6	[7]
Ni5P4	HER	10	114 mV	1MKOH	34	[8]
Ni5P4/NiP2/Ni2P	HER	10	120 mV	0.5MH2SO4	47.3	[9]
Cuf@ Ni5P4	HER	10	90 mV	0.5MH2SO4	49	[10]
WS2/ Ni5P4- Ni2P	HER	10	90 mV	0.5MH2SO4	74	[11]
Ni5P4-Ru	HER	10	54 mV	1MKOH	52	[12]
Co-doped (6.6at.%) Ni5P4	HER	10	310 mV	0.5MH2SO4	90	[13]
CC@Ni-P	HER	10	93 mV	0.5MH2SO4	58.2	[14]
Ni2P/Ni5P4@3DNG	HER	10	139 mV	0.5MH2SO4	59	[15]
Ni5P4/Ni2PFeNi@C	OER	10	242 mV	1MKOH	46	[16]
Co doping (i.e., 20%)- Ni5P4	HER	10	100.5 mV	1MKOH	65.8	[17]
Ni5P4/C	HER	10	103 mV	0.5MH2SO4	51	[18]
MF-GrCNTs-Se-Ni5P4	HER	10	130 mV	0.5MH2SO4	98	[19]

Table S3 Summary of various nickel phosphide catalytic electrodes for overall water splitting

Catalyst	Activity	Current density (mA/cm^2)	Potential	Electrolyte	Reference

3D SHF-Ni_5P_4	HER	10	106 mV	1 M KOH	This work
	OER	10	180 mV		
	Water plitting	10	1.47V		
$Ni_{0.975}Fe_{0.025}P$@CC	HER	10	131 mV	1 M KOH	[20]
	HER	100	257 mV		
	Water plitting	10	1.50 V		
S-doped Ni-P	HER	10	55		[21]
	OER	10	229		
	Water splitting	10	1.51V		
Fe-Ni_5P_4/NiFeOH-	HER	10	197 mV	1 M KOH	[22]
350	OER	10	221 mV		
	Water plitting	10	1.55 V		
Zn/F NiCoP/NF	HER	10	59		[23]
	OER	10	285		
	Water splitting	10	1.568		
NixPy-325	HER	20	160 mV	1 M KOH	[24]
	OER	10	320 mV		
	Water plitting	10	1.57V		
D- Ni_5P_4│Fe	HER	10	94.5 mV	1 M KOH	[25]
	OER	10	217 mV		
	Water plitting	10	1.59 V		
$Ni_2P/NiMoP_2$/CC	HER	10	102		[26]

	OER	10	230	
	Water splitting	10	1.59	
A-Ni_2P/Cu_3P	HER	10	88	[27]
	OER	10	262	
	Water splitting	10	1.60	
Fe, Rh- Ni_2P/NF	HER	10	73	[28]
	OER	30	226	
	Water splitting	10	1.62	

Reference

1 L. Zhang, C. Chang, C. W. Hsu, C. W. Chang and S.Y. Lu, J. Mater. Chem. A., 2017, 537, 19656-19663.

2 M. Ledendecker, S. K. Calderon, C. Papp, H.P. Steinruck, M. Antonietti and M. Shalom, Angew. Chem. Int.Ed., 2015, 54, 12361-12365.

3 G Wang, Y.V. Kolen'ko, X.Q. Bao, K. Kovnir and L. F. Liu, Angew. Chem. Int.Ed.,2015, 5428, 8188-8192.

4 K. Mishra, H. Q. Zhou, J. Y. Sun, F. Qin, K. Dahal, J. M. Bao, S. Chen and Z. F. Ren, Energy. Environ. Sci., 2018, 11, 2246-2252.

5 G. Lai, X. B. Liu, Y. Q. Deng, H. Yang, H. H. Jiang, Z. C. Xiao and T. Liang, Inorg. Chem. Commun., 2018, 97, 98-102.

6 Zhang, K. N. Yang, C. Wang, S. Y. Li, Q. Zhang, X. J Chang, J. Y. Li, S. M. Li, S. F. Jia, J. B. ang and L. Fu, Advan. Energy. Mater., 2018,829,1801690.

7 F. Chang, K. Li, Z. J. Wu, J. J. Ge, C, P, Liu and W. Xing, ACS Appl. Mater. Interface., 2018,1031,26303-26311.

8 C.S. Jung, K. Park, Y. R. Lee, I.H. Kwak, I.S. Kwon, J. D. Kim, J. Seo, J.P. Ahn and J. G. Park, CrystEngComm, 2019, 21, 1143-1149.

9 C. Hu, J. G. Cai, S. Liu, C. Lv, J. H. Luo, M. Duan, C. G. Chen, Y. Shi, J. F.Song, Z. Zhang, A. Watanabe, E. Aoyagi and S. Ito, ACS Appl. Energy Mater., 2019, 31, 1036-1045.

10 M. Das, N. Jena, T. Purkait, N. Kamboj, A. De Sarkar and R.S. Dey, J. Mater. Chem. A., 2019, 7, 23989-23999.

11 S. H. Yu, W. Z. Chen, H. Y. Wang, H. Pan and D. H. C. Chua, Nano Energy, 2019, 55, 193-202.

12 Q. He, D. Tian, H. L. Jiang, D. F. Cao, S. Q. Wei, D. B. Liu, P. Song, Y. Lin and L. Song, Adv. Mater., 2020, 3211, 1906972.

13 X. Xiao, X. J. Wu, Y. H. Wang, K. Zhu, B. T. Liu, X. Q. Cai, T. Yang, X. Y. Xu and D. G. Zhang, Catal. Commun.,

2020, 138, 105957.

14 A. Y. Chen, L. Fu, W. J. Xiang, W. Wei, D. Liu and C. L. Liu, Int. J. Hydrogen Energy., 2021, 46, 11701-11710.

15 G. S. Ding, Y. X. Zhang, J. Dong and L. B. Xu, Mater. Lett.,2021,299, 130071.

16 X. Y. Tian, P. Yi, J. W. Sun, C. Y. Li, R. Z. Liu and J.K. Sun, Nanomaterials, 2022, 1211, 1848.

17 C. C. Miao, Y. M. Zang, H. Wang, X. M Zhuang, N. Han, Y. X. Yin, Y. D Ma, M. Chen, Y. Dai, S. P. Yip, J.C. Ho and Z. X. Yang, Adv. Mater. Interfaces., 2022, 9, 2200739.

[18 H. M. Li, S.Q. Lu, J. Y. Sun, J. J. Pei, D. Liu, Y. R. Xue, J. J. Mao, W. Zhu and Z. B. Zhuang, Chem. Eur. J., 2018, 2445, 11748-11754.

19 M. Pahuja, S. Riyajuddin, M. Afshan, S. A. Siddiqui, J. Sultana, T. Maruyama and K. Ghosh, ACS Appl. Nano Mater., 2022, 51, 1385-1396.

20 T. G. Ma, Y. F. Qiu, Y. Y. Zhang, X. Y Ji and P. A. Hu, ACS Appl. Energy. Mater., 2019, 25, 3091-3099.

21 M. A. Ashraf, Y. f. Yang, D. Q. Zhang and B. T. Pham, J. Colloid. Interface. Sci., 2020, 577, 265-278.

22 C. F. Li, J. W. Zhao, L. J. Xie, J. Q. Wu and G. R. Li, Appl. Catal. B Environ., 2021, 291, 119987.

23 J. J. Zhu, X. Y. Zheng, C. C. Liu, Y. K. Lu, Y. Liu, D. Li and D. L. Jiang, J. Colloid. Interface. Sci., 2023, 630, 559-569.

24 J. Y. Li, J. Li, X. M. Zhou, Z. M. Xia, W. Gao, Y. Y. Ma and Y. Q. Qu, ACS Appl. Mater. Interfaces., 2016, 817, 10826-10834.

25 J. L. Qi, T. X. Xu, J. Cao, S. Guo, Z. X. Zhong and J. C. Feng, Nanoscale, 2020, 1210, 6204-6210.

26 J. H. Lin, Y. T. Yan, T. X. Xu, J. Cao, X. H. Zheng, J. C. Feng and J. L. Qi, J. Colloid. Interface. Sci., 2020, 564, 37-42.

27 L. Sun, S. T. Zhao, L. N. Sha, G. L. Zhuang, X. J. Wang and X. G. Han, J. Colloid. Interface. Sci., 2023, 637, 76-84.

28 T. Chen, J. J. Duan, J. J. Feng, L. P. Mei, Y. Jiao, L. Zhang and A. J. Wang, J. Colloid. Interface. Sci., 2022, 605, 888-896.

29 T. Shinagawa, A. Garcia-Esparza, K. Takanabe, Sci. Rep., 2015, 5, 13801

30 Z. Li, B. Li, M. Yu, C. Yu and P. Shen, International Journal of Hydrogen Energy, 2022, 47, 26956-26977